

Article

Full-Chain FeCl₃ Catalyzation Is Sufficient to Boost Cellulase Secretion and Cellulosic Ethanol along with Valorized Supercapacitor and Biosorbent Using Desirable Corn Stalk

Jingyuan Liu ^{1,2,3}, Xin Zhang ^{1,4}, Hao Peng ^{1,2}, Tianqi Li ^{1,2}, Peng Liu ^{1,2}, Hairong Gao ^{1,2}, Yanting Wang ^{1,2}, Jingfeng Tang ² , Qiang Li ³ , Zhi Qi ⁵, Liangcai Peng ^{1,2} and Tao Xia ^{1,4,*}

- ¹ Biomass & Bioenergy Research Center, College of Plant Science & Technology, Huazhong Agricultural University, Wuhan 430070, China
- ² Key Laboratory of Fermentation Engineering (Ministry of Education), National “111” Center for Cellular Regulation & Molecular Pharmaceutics, Cooperative Innovation Center of Industrial Fermentation (Ministry of Education & Hubei Province), College of Biotechnology & Food Science, Hubei Key Laboratory of Industrial Microbiology, Hubei University of Technology, Wuhan 430068, China
- ³ College of Engineering, Huazhong Agricultural University, Wuhan 430070, China
- ⁴ College of Life Science, Huazhong Agricultural University, Wuhan 430070, China
- ⁵ State Key Laboratory of Herbage & Endemic Crop Biotechnology, School of Life Sciences, Inner Mongolia University, Hohhot 010070, China
- * Correspondence: xiatao@mail.hzau.edu.cn; Tel.: +86-27-8728-1765; Fax: +86-27-8728-0016

Abstract: Cellulosic ethanol is regarded as a perfect additive for petrol fuels for global carbon neutralization. As bioethanol conversion requires strong biomass pretreatment and overpriced enzymatic hydrolysis, it is increasingly considered in the exploration of biomass processes with fewer chemicals for cost-effective biofuels and value-added bioproducts. In this study, we performed optimal liquid-hot-water pretreatment (190 °C for 10 min) co-supplied with 4% FeCl₃ to achieve the near-complete biomass enzymatic saccharification of desirable corn stalk for high bioethanol production, and all the enzyme-undigestible lignocellulose residues were then examined as active biosorbents for high Cd adsorption. Furthermore, by incubating *Trichoderma reesei* with the desired corn stalk co-supplied with 0.05% FeCl₃ for the secretion of lignocellulose-degradation enzymes in vivo, we examined five secreted enzyme activities elevated by 1.3–3.0-fold in vitro, compared to the control without FeCl₃ supplementation. After further supplying 1:2 (*w/w*) FeCl₃ into the *T. reesei*-undigested lignocellulose residue for the thermal-carbonization process, we generated highly porous carbon with specific electroconductivity raised by 3–12-fold for the supercapacitor. Therefore, this work demonstrates that FeCl₃ can act as a universal catalyst for the full-chain enhancement of biological, biochemical, and chemical conversions of lignocellulose substrates, providing a green-like strategy for low-cost biofuels and high-value bioproducts.

Keywords: metal catalyst; biomass saccharification; electroconductivity; cellulase secretion; corn stalk



Citation: Liu, J.; Zhang, X.; Peng, H.; Li, T.; Liu, P.; Gao, H.; Wang, Y.; Tang, J.; Li, Q.; Qi, Z.; et al. Full-Chain FeCl₃ Catalyzation Is Sufficient to Boost Cellulase Secretion and Cellulosic Ethanol along with Valorized Supercapacitor and Biosorbent Using Desirable Corn Stalk. *Molecules* **2023**, *28*, 2060. <https://doi.org/10.3390/molecules28052060>

Academic Editors: Francesco Enrichi, Alberto Vomiero and Elti Cattaruzza

Received: 25 January 2023

Revised: 16 February 2023

Accepted: 17 February 2023

Published: 22 February 2023



Copyright: © 2023 by the authors. Licensee MDPI, Basel, Switzerland. This article is an open access article distributed under the terms and conditions of the Creative Commons Attribution (CC BY) license (<https://creativecommons.org/licenses/by/4.0/>).

1. Introduction

Lignocellulose is the most renewable biomass resource on Earth; it is convertible into bioethanol and bioproduction for reduced net-carbon release [1,2]. For bioethanol processes, three major steps are principally required, including biomass pretreatment for lignocellulose deconstruction, sequential enzymatic hydrolysis for fermentable sugars and final yeast fermentation for ethanol production [3,4]. However, the intrinsic recalcitrance of lignocellulose leads to highly costly pretreatments and low-efficiency enzymatic saccharification [5], which is unacceptable for large-scale cellulosic ethanol production with potential secondary-waste release into the environment [6]. Hence, the use of green-like technology for cost-effective biofuels and high-value bioproducts remains to be explored.

Lignocellulose recalcitrance is principally formed by distinct cell-wall composition, characteristic wall-polymer features, and dense wall-network interlinks. To reduce recalcitrance, various physical and chemical pretreatments have been broadly conducted with diverse lignocellulose resources [7,8]. Although chemical pretreatments can extract partial wall polymers (hemicellulose, lignin) and alter cellulose features (crystallinity, polymerization) to increase lignocellulose accessibility, they mostly require high temperatures and high concentrations, along with additional processes for chemical recycling. Alternatively, liquid-hot-water pretreatment is applicable as a non-chemical and green-like biomass process [9], but its effectiveness is restricted for largely enhanced biomass enzymatic hydrolysis [10].

For the sequential enzymatic hydrolysis of pretreated lignocellulose residues, mixed cellulases are commonly utilized by incubating *Trichoderma reesei* with a desirable biomass substrate as a carbon source for enzyme secretion [11]. In principle, the *T. reesei*-secreted cellulases are the complexes of three different major enzymes: exoglucanase (CBH), endoglucanase (EG), and β -glucosidase (BG). In particular, advanced biotechnology is increasingly explored to improve the *T. reesei* strain secretion of cellulases and xylanases with high activities [12].

In the full utilization of lignocellulose, the remaining biomass residues obtained from enzymatic hydrolysis and yeast fermentation are considered to generate value-added biochar and nanocarbon via thermal–chemical conversion [13,14]. As biocarbon has a stable structure, large specific surface area, and pore volume, it has been widely employed for environmental remediation and electroconductivity [15,16]. Importantly, iron chemicals, such as K_2FeO_4 and $FeCl_3$, have been supplied as graphitization agents for synchronous activation with pyrolysis to generate graphitic carbons [17–19]. Although iron-based catalysts have been implemented to enhance biochemical and thermal–chemical processes of lignocellulose substrates, most iron chemicals are reported to be inhibitors of biomass enzymatic saccharification and the secretion of fungi by cellulases [20]. However, ferric ions are essential for living organisms; they generally produce high-affinity iron-chelating compounds to scavenge the metal necessary for their metabolism [21]. In particular, the presence of chloride could increase cellulase activity [22].

Corn is a highly photosynthetic-efficient C4 crop that annually produces billions of tons of grain and lignocellulose residues [23]. Using the mature stalks of two distinct corn cultivars (Huatiannuo-3/ZH and Xianyu-1171/ZX), in this study, we performed optimal liquid hot water (LHW) pretreatments that were co-supplied with low dosages of $FeCl_3$ as the active catalyst to distinctively extract wall polymers for significantly improved lignocellulose recalcitrance, which led to the achievement of near-complete biomass enzymatic saccharification for high bioethanol production in the desired corn cultivar (ZH) [24]. By collecting all the solid lignocellulose residue obtained from the enzymatic hydrolysis, in this study, we examined its adsorption capacity with Cd as the active biosorbent [25]. Meanwhile, the raw stalk of the desired corn cultivar (ZH) was also used as a carbon source to incubate with the *Trichoderma reesei* for secreting high-activity lignocellulose-degradation enzymes by co-supplying low dosages of $FeCl_3$ for *T. reesei* cultivation. After harvesting all the supernatants containing the mixed cellulases and xylanases secreted by the *T. reesei* strain, all the remaining lignocellulose residues were also processed to generate graphitic carbon by a classic thermal–chemical reaction co-supplied with 1:2 (*w/w*) $FeCl_3$ as the catalyst, and the porous carbon was further examined for electroconductivity [13]. Hence, this study demonstrates the multiple roles of $FeCl_3$ as a sensitive catalyst enabling the improvement of two full-chain biomass processes for cost-effective biofuels and highly valuable bioproducts with zero biomass-waste release.

2. Results and Discussion

2.1. Enhanced Biomass Saccharification of Corn Stalks for Bioethanol Production under Optimal LHW Pretreatment with $FeCl_3$ Co-Supplement

As generally described for all the experiments conducted in this study (Figure S1), we initially collected the mature stalks of two corn cultivars (ZH and ZX) with distinctive

cell-wall compositions (Table 1). In general, the ZH stalk consisted of significantly lower lignin and cellulose levels than those of the ZX at the $p < 0.01$ level ($n = 3$), with similar hemicellulose contents. In particular, the ZH stalk contained more soluble sugars, which should be directly fermentable for bioethanol production. Next, this study performed various liquid hot water (LHW) pretreatments co-supplied with low dosages of FeCl_3 as the catalyst to enhance sequential-biomass saccharification by measuring the hexose yield released from enzymatic hydrolysis (Figure 1). During the LHW pretreatment at 190°C for 10 min, 4% FeCl_3 co-supplement was effective for enhancing biomass enzymatic saccharification in two corn cultivars, and the highest hexose yields at 70% and 95% (% cellulose) were achieved while the LHW temperature was as high as 190°C (Figure 1A–C). Although the optimal LHW pretreatment (190°C for 10 min) led to increases in the hexose yields of 1.7- and 1.8-folds in two corn cultivars relative to their raw samples (without pretreatment), the 4% FeCl_3 co-supplement increased the hexose yields by as much as 3.0- and 4.4-fold (Figure 1D), suggesting that FeCl_3 catalysis should play much more enhancement roles for biomass enzymatic saccharification in corn stalks. Consistently, the ZH cultivar displayed significantly higher biomass saccharification than that of the ZX, including both hexoses and total sugar yields (Figure 1E), indicating that the lignocellulose substrate of the ZH stalk has relatively few recalcitrant properties. Furthermore, this study performed yeast fermentation by using all the hexoses released from the enzymatic hydrolysis of the pretreated lignocellulose substrate, and the 4% FeCl_3 co-supplement caused the highest bioethanol yields, of 9.13% and 11.24% (% dry matter), in the two corn cultivars upon the optimal LHW pretreatments (Figure 1F), which were consistent with their increased hexose yields. In addition, the mass-balance analysis revealed that integrating the LHW pretreatments with low-dosage- FeCl_3 catalysis was effective for wall polymer (lignin, hemicellulose) extraction, leading to near-complete biomass enzymatic saccharification and higher bioethanol production in the desired corn (ZH) cultivar (Figure S2). Therefore, the optimal LHW pretreatment co-supplied with 4% FeCl_3 can not only provide a relatively cost-effective and green-like biomass process approach, but it may also demonstrate that FeCl_3 is an efficient catalyst for lessening lignocellulose recalcitrance.

Table 1. Cell-wall compositions (% dry matter) of two corn (ZX, ZH) cultivars.

Samples	Wall Polymer Level (% Dry Matter)			
	Cellulose	Hemicellulose	Lignin	Soluble Sugar
ZX	32.63 ± 1.49	17.82 ± 0.06	16.7 ± 0.38	17.77 ± 0.38
ZH	$26.37 \pm 0.60^{**}$	$19.30 \pm 0.26^{**}$	$13.05 \pm 0.63^{**}$	$22.87 \pm 0.94^{**}$

** A significant difference between ZX and ZH samples at $p < 0.01$ level ($n = 3$).

2.2. Improved Lignocellulose Recalcitrance from FeCl_3 Catalysis in Corn Stalks

To understand why the 4% FeCl_3 supplement with optimal LHW pretreatment could largely extract wall polymers (lignin, hemicellulose) for significantly enhanced biomass enzymatic saccharification, as described above (Figures 1 and S2), we further conducted the Fourier transform infrared (FT-IR) spectroscopic profiling of pretreated lignocelluloses in two corn stalks (Figure 2A,B). As a result, several typical peaks corresponding for the functional groups (C-O-C [26,27], C-H [28–30], C-O [31], O-H [31]) associated with wall-polymer interactions were relatively altered in the LHW-pretreated lignocelluloses, particularly for the FeCl_3 -catalyzed substrates (Table S1), confirming distinct wall-polymer extraction from the optimal LHW pretreatment co-supplied with FeCl_3 . As a consequence, significantly raised cellulose CrI values were detected in the optimal LHW-pretreated residues with 4% FeCl_3 catalysis (Figure 2C), which could explain the significantly higher wall-polymer extraction via the disassociation of hydrogen bonds with cellulose microfibrils in the two corn cultivars [32]. Although the optimal LHW pretreatments significantly reduced the cellulose DP values at the $p < 0.01$ level ($n = 3$) compared to their raw materials (without pretreatment), the 4% FeCl_3 co-supplement led to the lowest cellulose DP values detected in the two corn cultivars (Figure 2D), which may explain why cellulose accessibility was mostly raised in the

LHW-pretreated residues with 4% FeCl₃ catalysis (Figure 2E) [33,34]. Using scan electron microscopy, we further observed much rougher surfaces of pretreated lignocellulose residues, particularly from the optimal LHW pretreatments co-supplied with 4% FeCl₃ (Figure S3), which was consistent with their remarkably increased cellulose accessibility. As cellulose accessibility is a direct parameter accounting for biomass enzymatic hydrolysis [35], the data obtained in this study demonstrate that 4% FeCl₃ catalysis is mostly effective at reducing lignocellulose recalcitrance for significantly enhanced biomass saccharification through optimal LHW pretreatment conducted in the two corn cultivars.

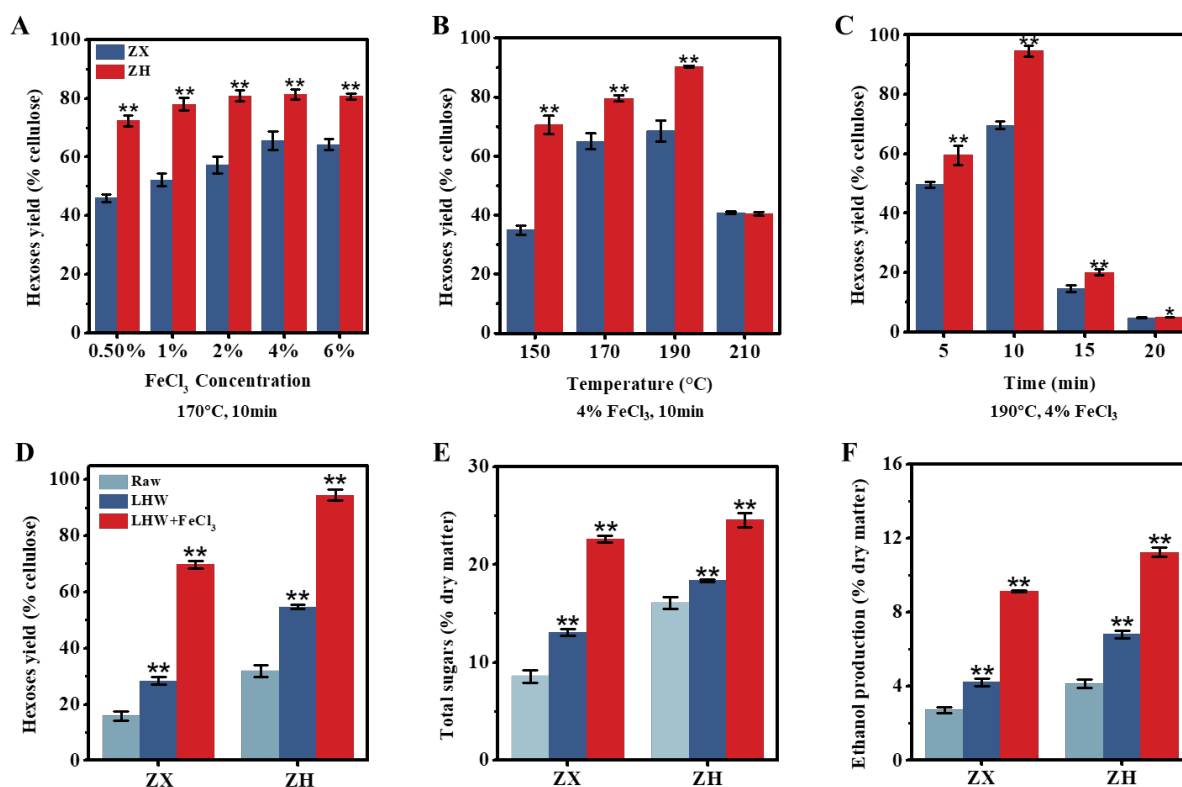


Figure 1. Optimal liquid hot water (LHW) pretreatment co-supplied with FeCl₃ for biomass enzymatic saccharification and bioethanol production in two corn (ZX, ZH) cultivars. (A–C) The LHW pretreatments under different conditions by measuring hexose yields released from enzymatic hydrolyses of pretreated residues; (D,E) hexose and total sugar yields under two pretreatments (optimal LHW at 190 °C for 10 min with/without 4% FeCl₃) relative to the control (raw material without pretreatment), total sugars calculated from all hexoses and pentoses released from enzymatic hydrolysis; (F) ethanol yield obtained from yeast fermentation by using all hexoses as carbon sources. Data as mean ± SD (*n* = 3); * or ** a significant difference between two corn cultivars (A–C) or pretreated residue and raw material at *p* < 0.05 or 0.01 level.

2.3. Enzyme-Undigestible Lignocellulose as Active Biosorbent for Cd Adsorption

Even though the desired corn cultivar (ZH) showed a near-complete biomass enzymatic saccharification under the optimal LHW pretreatment co-supplied with 4% FeCl₃, this study collected all the enzyme-undigestible solid-lignocellulose residue to detect its adsorption capacity with Cd using our recently established approach [25,36]. Compared with the residue obtained from the direct enzymatic hydrolysis of the desired corn stalk (without pretreatment), the enzyme-undigestible residue after the optimal LHW pretreatment showed significantly reduced Cd adsorption, by 1.5-fold, at the *p* < 0.01 level (Figure 3). However, the undigestible residue from the optimal LHW pretreatment co-supplied with 4% FeCl₃ was of the highest Cd adsorption capacity among the three residue samples examined, which was almost 1.9-fold higher than that of the residue from the optimal LHW pretreatment only. Therefore, integrating optimal LHW pretreatment with 4% FeCl₃

catalysis not only mostly reduced the lignocellulose recalcitrance for the increased biomass enzymatic saccharification, but also its undigestible residue was fully applicable as an active biosorbent for high Cd adsorption without any zero-biomass-waste release.

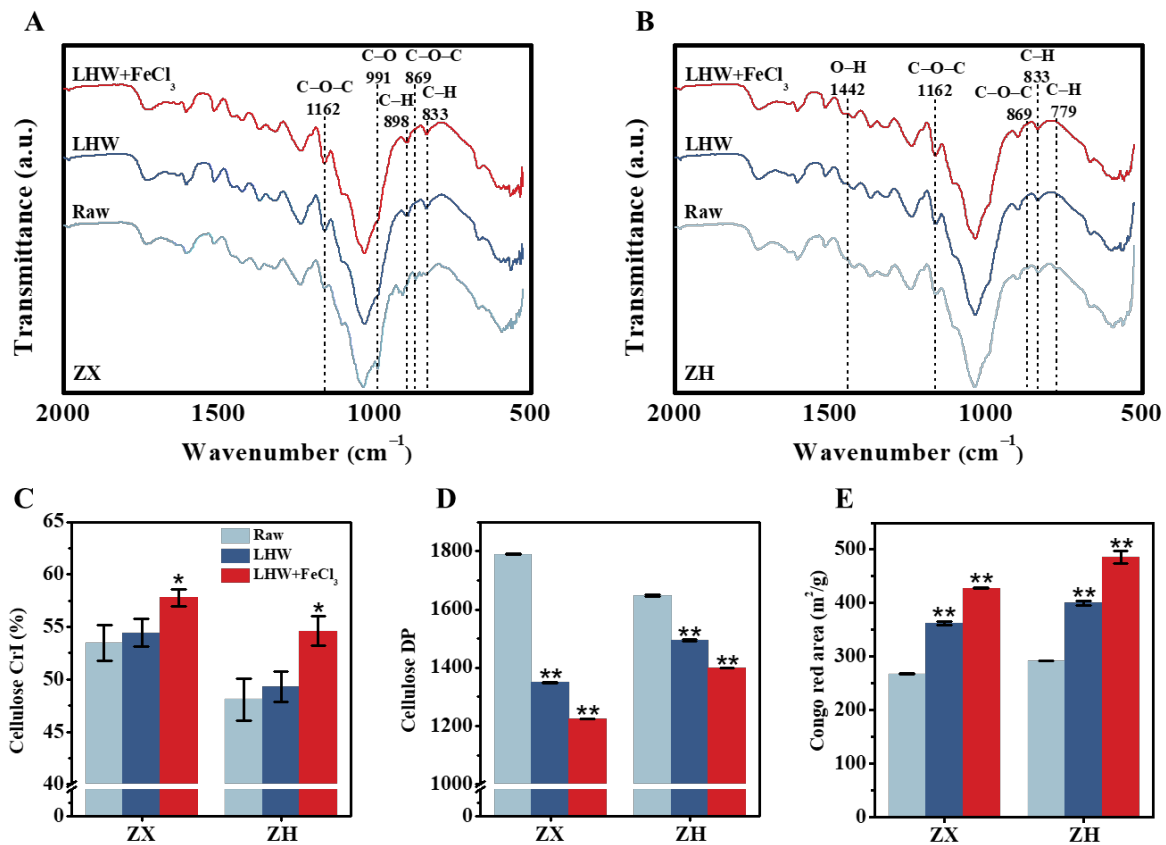


Figure 2. Characterization of wall-polymer linkages and cellulose features after optimal LHW pretreatment co-supplied with 4% FeCl₃ in two corn cultivars. (A,B) Fourier transform infrared (FT-IR) spectroscopic profiling, as annotated in Table S1; (C,D) cellulose CrI and DP; (E) cellulose accessibility by Congo red staining. Data as mean ± SD (*n* = 3); * or ** a significant difference between pretreated residue and raw material at *p* < 0.05 or 0.01 level.

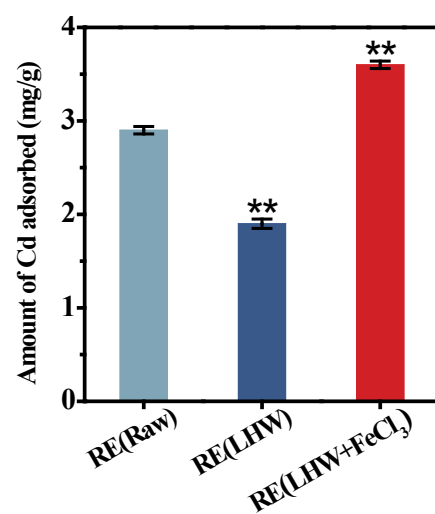


Figure 3. The Cd-adsorption capacity with the enzyme-undigestible residues as biosorbent upon the optimal LHW pretreatment co-supplied with/without 4% FeCl₃ in the desirable corn (ZH) cultivar. Data as mean ± SD (*n* = 3); ** a significant difference between pretreated residues and raw material at *p* < 0.01 level.

2.4. FeCl₃ Supplement for Upgraded Lignocellulose-Degradation-Enzyme Activity Secreted by *T. reesei* Incubation with Corn Stalk

As FeCl₃ acts as an efficient catalyst for reducing the lignocellulose recalcitrance of the desired corn stalk during the LHW pretreatment performed above, we attempted to test the other role of FeCl₃ in enhancing the *T. reesei* secretion of lignocellulose-degradation enzymes. Using our recently established approach [37,38], the raw material of the corn ZH stalk was incubated in vivo with *T. reesei* as the carbon source co-supplied with FeCl₃ at different concentrations (0.01%, 0.05%, 0.1%), and the supernatants were then collected for enzyme-activity assay in vitro (Figure 4). As a comparison with the control (without FeCl₃), the 0.05% FeCl₃ supplement led to significantly raised enzyme activities, by 1.3–3.0 fold, for all five assays of the *T. reesei* secretion (Figure 4A–E), indicating that FeCl₃ can act as an active biological catalyst for fungi secretion from multiple cellulases and xylanase. However, while a high concentration (0.1%) of FeCl₃ was supplied to the *T. reesei* incubation, three enzyme activities (filter paper, β-glucosidase, xylanase) were deeply inhibited and only CBH activity and EG activity remained slightly high relative to the control. Meanwhile, the FeCl₃ supplement at the extremely low concentration (0.01%) only significantly raised the CBH activity and xylanase activity, but it also led to higher total protein production (Figure 4F), suggesting that *T. reesei* secretion could be sensitive to FeCl₃ catalysis during its incubation with lignocellulose substrate. Notably, this study compared these five enzyme-activity assays with the previously reported assays enhanced by supplying Mn²⁺ or Co²⁺ or Ca²⁺ in fungal incubation [39–41], and the 0.05% FeCl₃ supplement enhanced the most enzyme activities examined in this study (Table 2). Based on the performance of SDS-PAGE, this study finally identified a total of 11 enzymes secreted by *T. reesei* incubation with the desired corn stalk co-supplied by 0.05% FeCl₃ (Table 3, Figure S4), which confirms the production of various cellulases and xylanases at high levels of activity secreted by *T. reesei*.

Table 2. Comparison of enzyme activities secreted by fungi co-supplied with various metals.

Inducing Substrate	Increased Enzymatic Activities (%)					Reference
	FPA	CBH	EG	BG	Xylanase	
Fe ³⁺	29.38	199.37	99.16	38.38	53.72	This study
Mn ²⁺	- *	94	62	-	-	[40]
Co ²⁺	-	-	58.62	-	-	[41]
Ca ²⁺	-	40	80	-	40	[39]

* The data are not available.

Table 3. The LC–MS/MS assay of *T. reesei*-secreted enzymes incubated with corn stalk and 0.05% FeCl₃.

Protein Name	Accession No.	iBAQ (×10 ⁶)	MW [kDa]
Exoglucanase I	P62694	3009	54.07
Endo-β-1,4-glucanase I	G0RKH9	656.77	48.21
Endo-β-1,4-glucanase II	G0RB67	44.16	254.04
Endo-β-1,4-glucanase VII	A0A024SFJ2	53.24	26.8
β-D-glucosidase	Q12715	50.95	78.43
β-glucosidase	G0RDY1	3.42	84.68
Endo-1,4-β-xylanase	A0A1L7H884	4144.40	20.77
Endo-1,4-β-xylanase I	P36218	189.98	24.58
Xyloglucanase	A0A024S9Z6	192.46	87.13
β-xylosidase	Q92458	238.57	87.19
β-xylanase	Q9P973	143.56	38.08

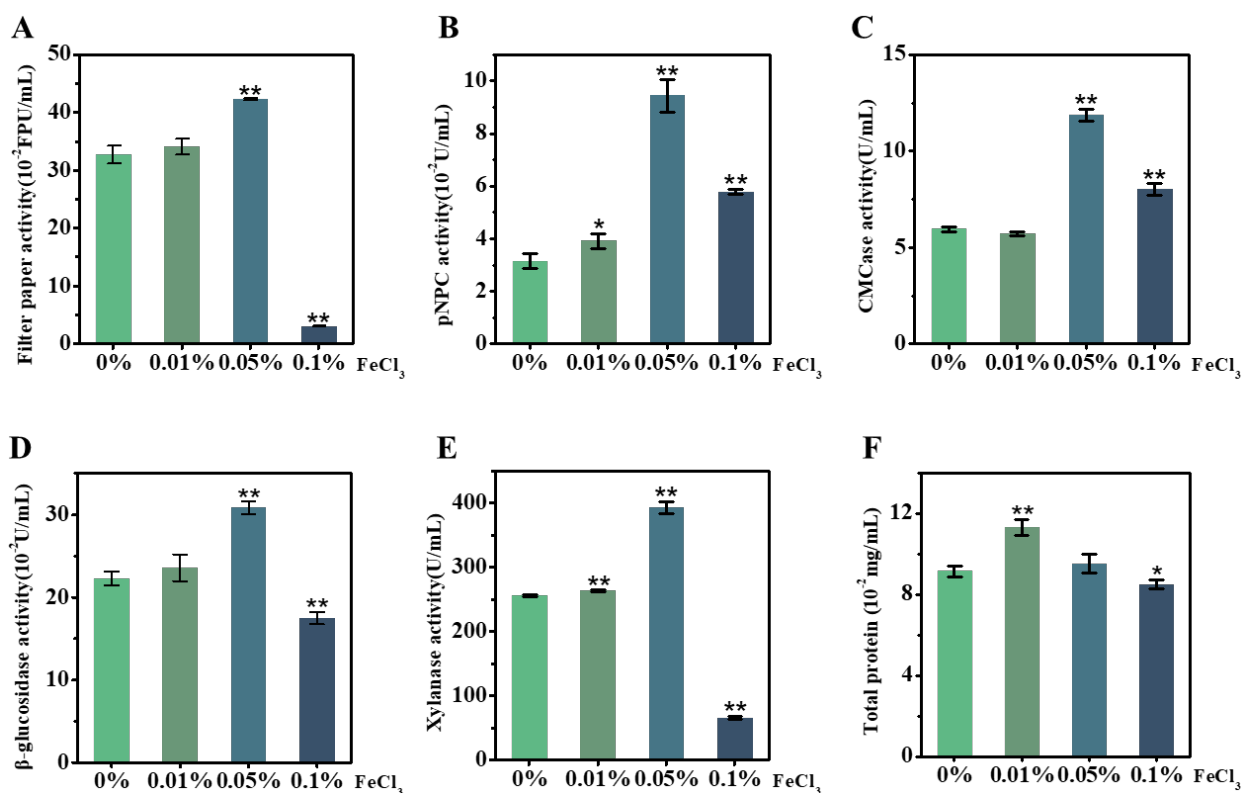


Figure 4. Activity assays in vitro of lignocellulose-degradation enzymes secreted by *T. reesei* incubation with raw stalk of ZH cultivar co-supplied with different concentrations of FeCl₃ in vivo. (A) Filter-paper activity; (B) CBH; (C) EG; (D) BG; (E) xylanase; (F) total protein of supernatant. Data as mean \pm SD ($n = 3$); * or ** a significant difference between FeCl₃-supplied samples and control (without FeCl₃) at $p < 0.05$ or 0.01 level.

2.5. Porosity-Raised Biocarbon Generated by FeCl₃ Activation with *T. reesei*-Undigested Lignocellulose Residues

Given that the *T. reesei* incubation co-supplied with 0.05% FeCl₃ led to high-activity enzyme secretion, as described above, a large amount of undigested lignocellulose residues remained. Hence, in this study, we further generated porous carbons by performing classic thermal-chemical conversion co-supplied with FeCl₃ at a proportion of 1:2 (w/w) into the *T. reesei*-undigested residue substrate of the desired corn stalk (Figure 5). Based on the BET assay by N₂ absorption, this study observed a typical sorption isotherm accountable for the presence of micro-pores in the carbon of the control *T. reesei*-undigested residue (without 1:2 FeCl₃ activation), whereas a small hysteresis loop under the medium-pressure range was found for the meso-pores in the *T. reesei*-undigestible residue activated by 1:2 FeCl₃ (Figure 5A), suggesting a distinct pore-size distribution of biocarbon activated by 1:2 FeCl₃ [42]. Furthermore, we found that the 1:2 FeCl₃ activation raised the porous volume much more than, and the specific surface area of the biocarbon twofold, compared with the control sample (Figure 5B,C), suggesting that FeCl₃ activation plays an enhancement role in the generation of highly porous biocarbon [18]. During the TEM observation, the FeCl₃-activated sample showed graphene-like carbon with fewer layers than that of the control sample (Figure 5D), which was consistent with its significantly increased porosity. The Raman scanning revealed a typical G-peak ($\sim 1580 \text{ cm}^{-1}$), which represented the graphene-like carbon generated in the FeCl₃-activated sample (Figure 5E) [43], and the XRD assay further confirmed two diffraction peaks at 24° and 44°, which were slightly shifted in relation to the diffraction peaks (2θ) for the (002) and (100) planes of the graphite (Figure 5F) [44,45]. However, the lack of a 2D peak in the Raman scanning suggested a relatively poor quality of graphene-like carbon. Furthermore, in this study, we applied

XPS to detect the element composition and chemical characteristics of the FeCl₃-activated sample (Figure 5G–I). As a result, the FeCl₃-activated sample mainly contained carbon (C) at 88.01% and oxygen (O) at 11.78% with tiny iron (Fe) at 0.14%, suggesting that the 1:2 FeCl₃ supplement mainly acted as a chemical catalyst for the generation of highly porous carbon (Figure 5G). Individual peaks were accordingly identified, such as sp²-bonded carbon (284.5 eV), sp³-C (285.0 eV), C-O (286.2 eV), C=O (288.1 eV) and O-C=O (288.9 eV) (Figure 5H) [46,47]. In addition, the XPS O 1s spectrum showed two major peaks corresponding to C=O (532.1 eV) and C-O (533.6 eV) (Figure 5I) [48], which may have served as the active sites for the high-porosity biocarbon generated in this study.

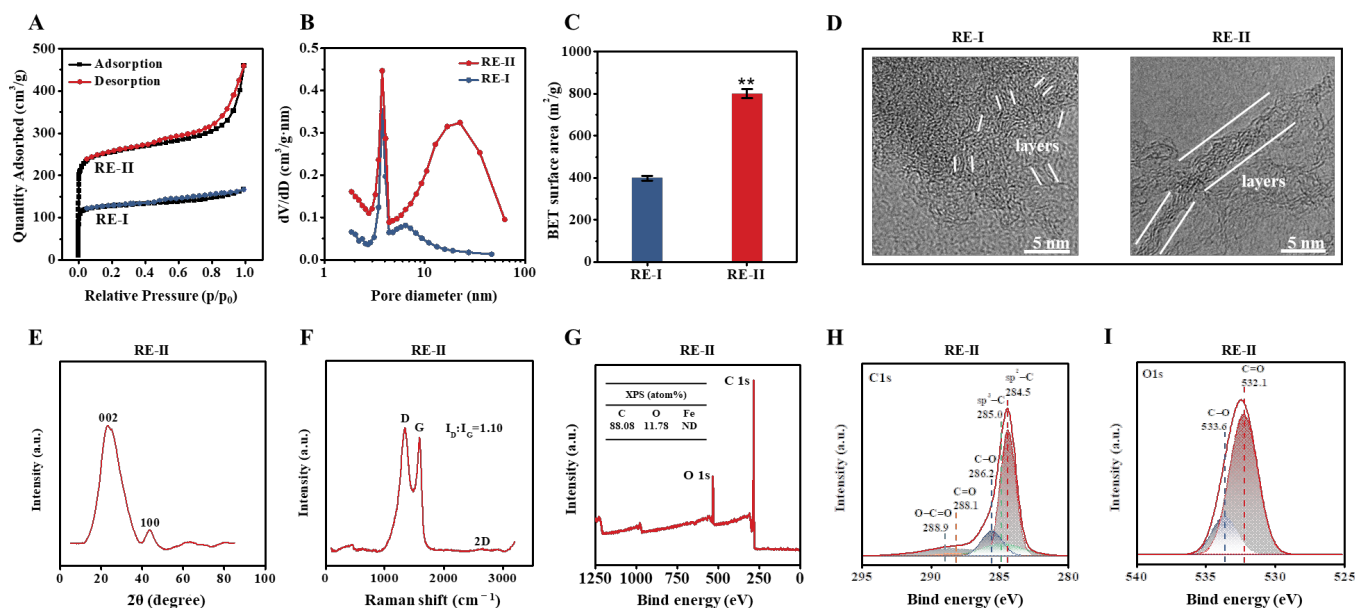


Figure 5. Characterization of the porous carbons generated by 1:2 (*w/w*) FeCl₃-activated thermal-chemical conversion of the lignocellulose residues (RE) from *T. reesei* incubation with raw ZH stalk co-supplied with 0.05% FeCl₃. (A–C) For the two carbon generated from RE-I (Raw + 0.05% FeCl₃) and RE-II (Raw + 0.05% FeCl₃) + 1:2 FeCl₃: (A) TEM observation; (B) nitrogen adsorption/desorption isotherm profiling; (C) pore-size-distribution profiling; (D) BET surface-area assay. (E–I) For the carbon sample generated from RE-II: (E) X-ray assay; (F) Raman-spectra profiling; (G) XPS-spectra profiling; (H,I) high-resolution XPS spectrum at C1s region and high-resolution XPS spectrum at O1s region (I). ** a significant difference between two lignocellulose residues at $p < 0.05$ or 0.01 level.

2.6. Improved Supercapacitor Performance of the Porous Carbon Generated by FeCl₃ Activation

Since the highly porous carbon was generated by 1:2 FeCl₃ activation with the *T. reesei*-undigested lignocellulose residues, as described above, this study tested its electrochemical performance using our previously established approaches [45]. In general, three types of carbon sample all displayed quasi-rectangular shapes, which represented the good character of the double-layer capacitor (Figures 6 and S5). However, during a comparison with the controls of the two carbon samples (without FeCl₃ for thermal-chemical conversion), the FeCl₃-activated carbon showed a higher current response at different scan rates for better capacitive properties, which were mainly due to its larger specific surface area and porous volume, as described above. Galvanostatic charge–discharge (GCD) tests were also conducted with three carbon samples, and a typical inverted “V” shape was observed, suggesting a classic capacitive response and fast charge transfer (Figure 6B). Consistently, the FeCl₃-activated carbon sample displayed a much longer discharging time for the highest specific capacitance in the electrolyte systems examined among the three carbon samples. Furthermore, the specific capacitances were evaluated by the discharge times at different current densities, and the FeCl₃-activated carbon sample showed much higher specific capacitances than those of the two control samples, by 3–12-fold (Figure 6C),

which confirmed that the 1:2 FeCl₃ supplement effectively catalyzed the thermal–chemical conversion of the *T. reesei*-undigested lignocellulose residues into highly porous carbon as the supercapacitor. Nevertheless, the specific capacitances of the FeCl₃-activated carbon sample remained lower than the carbons generated from other biomass resources, according to previous reports [17,49–51], indicating that optimal FeCl₃ activation should be explored in future studies. In addition, of the two controls, the carbon sample generated from the *T. reesei*-undigested residues co-supplied with 0.05% FeCl₃ also displayed consistently higher electroconductivity than that of the carbon sample without the 0.05% FeCl₃ supplement, which suggests that the 0.05% FeCl₃ supply was also effective at improving the production of *T. reesei*-incubated lignocellulose residue for the generation of highly porous carbon.

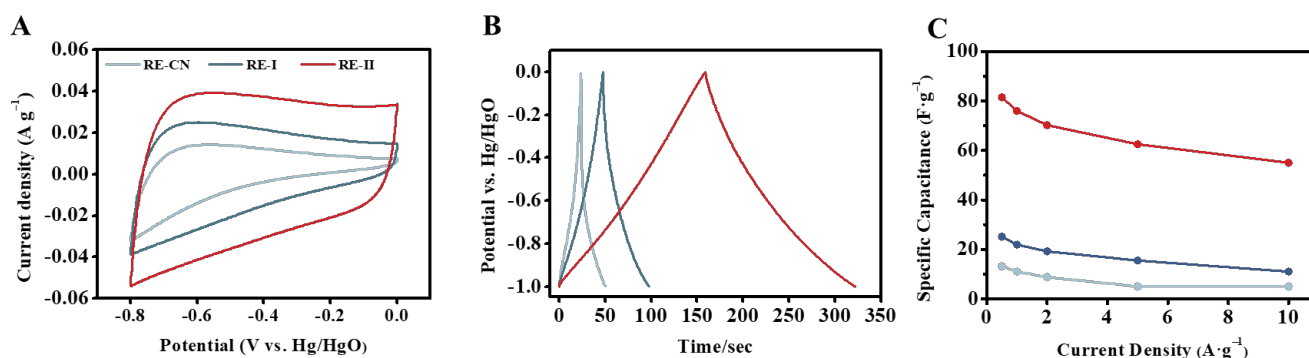


Figure 6. Electrochemical properties of the porous carbon generated by 1:2 (*w/w*) FeCl₃-activated thermal–chemical conversion of the lignocellulose residues (RE) from *T. reesei* incubation with raw ZH stalk co-supplied with 0.05% FeCl₃. (A–C) For the three carbon samples generated from RE-I (Raw + 0.05% FeCl₃), RE-II (Raw + 0.05% FeCl₃) + 1:2 FeCl₃ and RE-CN (raw, incubated with *T. reesei* without FeCl₃): (A) Cyclic-voltammety curves at 100 mV s⁻¹; (B) galvanostatic charge/discharge curves at 0.5 A/g; (C) specific capacitance calculated by galvanostatic charge–discharge at different current densities.

3. Materials and Methods

3.1. Collection of Mature Stalks in Two Corn Cultivars

Two corn cultivars (Huatiannuo-3/ZH and Xianyu-1171/ZX) were grown in the Experimental Field of Huazhong Agricultural University. The mature stalks of two corn cultivars were collected, dried at 50 °C, and ground into the powders through a 40-mesh screen. The soluble sugars of corn stalks were extracted with potassium-phosphate buffer (0.5 M, pH 7.0); the solid residues were rinsed with deionized water until reaching pH 7.0, dried, and stored in a dry container until use.

3.2. Wall-Polymer Extraction and Determination

Wall-polymer extraction and assay were conducted as previously described [52], with minor modifications [53]. Total lignin was measured by the Laboratory Analytical Procedure of the National Renewable Energy Laboratory with minor modification [54]. All assays were completed in independent triplicates.

3.3. Detection of Wall-Polymer Features

The degree of polymerization (DP) and crystalline index (CrI) of cellulose samples were detected as previously described [55]. Cellulose accessibility was estimated by performing Congo red (CR) staining as described in [56], with minor modifications [55]. Monosaccharides of hemicellulose were analyzed by GC-MS (SHIMADZU GCMS-QP2010 Plus, Berlin, Germany), as described in [57].

3.4. Lignocellulose Observation and Characterization

Biomass morphology was observed under scanning electron microscopy (SEM, Gemini 500, Obercohen, Germany), as previously described [8]. Lignocellulose chemical linkages were detected by Fourier transform infrared (FT-IR) method (Thermo Fisher Scientific, Waltham, MA, USA), as described in [58].

3.5. Liquid Hot Water (LHW) Pretreatment Co-Supplied with FeCl_3

The biomass samples (0.300 g) were mixed with 2.4 mL FeCl_3 at various concentrations (0.5%, 1%, 2%, 4% and 6% *w/v*). The well-mixed samples were placed into stainless-steel bomb with PTFE jars and a thermostatic magnetic stirrer (Kerui Instrument Co., Ltd., Gongyi, China) under shaking at 60 rpm. The samples were incubated at 150 °C, 170 °C, 190 °C and 210 °C for 5 min, 10 min, 15 min and 20 min, respectively. After reactions, the bombs were cooled to room temperature, the pretreated samples were rinsed several times with deionized water until pH 7.0, and the remaining solid residues were collected for enzymatic hydrolysis. All assays were conducted in independent triplicates.

3.6. Enzymatic Hydrolysis and Yeast Fermentation for Bioethanol Production

The pretreated lignocellulose residues were rinsed with potassium-phosphate buffer (0.2 M, pH 4.8) and then incubated under 5% (*w/v*) solid loading with 6 mL (2.0 g/L) of mixed cellulases (HSB, containing cellulases at 13.25 FPU/g biomass and xylanase at 8.40 U /g biomass from Imperial Jade Bio-technology Co., Ltd., Yinchuan, China) for 48 h under shaking at 150 rpm, at 50 °C, and co-supplied with 1% (*v/v*) Tween-80. After centrifugation at $4000 \times g$ for 5 min, the supernatants were collected for hexose and pentose assay, and the solid residuals were collected for Cd-adsorption assay.

Yeast fermentation and ethanol measurement were conducted as previously described [59]. About 0.5 g/L of *Saccharomyces cerevisiae* (Angel Yeast Co., Ltd., Yichang, China) was incubated with the supernatants collected from enzymatic hydrolyses of pretreated lignocellulose residues, and the fermentation was conducted at 37 °C for 48 h. Ethanol was measured using the $\text{K}_2\text{Cr}_2\text{O}_7$ method [60]. All assays were conducted in independent triplicates.

3.7. Cd-Adsorption Analysis

The solid residues remaining from enzymatic hydrolysis were washed with ultra-pure water and dried as biosorbent for Cd-adsorption analysis, as previously described [36]. Solution of 5 mg/L Cd^{2+} was prepared by adding $\text{Cd}(\text{NO}_3)_2 \cdot 4\text{H}_2\text{O}$ into ultra-pure water. The adsorption experiment with 0.025 g biosorbent was performed in 50-milliliter tubes for 4 h under shaking at 150 rpm. After the adsorption experiment, the samples were filtered through a 0.45-micrometer-membrane filter, and the residual Cd^{2+} concentration in the filtrate was detected by flame atomic adsorption spectrophotometer (FAAS HITACHI Z-2000, Tokyo, Japan) equipped with air-acetylene flame, as previously described [36]. The Cd adsorption at equilibrium q_e (mg/g) and the percentage removal efficiency (%R) were estimated as described in [61].

3.8. *T. reesei* Strain Cultivation Induced by FeCl_3 and Enzyme-Activity Determination

The *T. reesei* Rut-C30 strain (CICC 40348, from China Center of Industrial Culture Collection) was grown on potato-dextrose agar (PDA) at 30 °C for 7 d, and the spores were harvested with double distilled water and counted on the hemocytometer. The germination rate of spores was accurately examined for appropriate incubation time prior to micro-fluidic analysis and sorting. The spores were collected and adjusted to a density of 1×10^7 spores/mL. A spore suspension of about 500 μL was added into 30 mL of liquid cellulase-inducing medium, incubated at 30 °C under shaking at 200 rpm for 7 d. The liquid cellulase-inducing medium was prepared as previously described [37]. About 0.6 g of biomass powder of corn stalk without soluble sugars was added into the liquid cellulase-

inducing medium as carbon source and induced by FeCl_3 at various concentrations (0%, 0.01%, 0.05%, and 1%; w/v).

Filter-paper activity (FPA) of crude cellulase solutions secreted by *T. reesei* was determined as described previously [37]. Exoglucanase (CBH), endoglucanase (EG), β -glucosidase (BG), and xylanase activities of crude cellulase solutions secreted by *T. reesei* were examined in vitro by using carboxymethylcellulose sodium (CMC-Na), 4-Nitrophenyl β -D-cellobioside (pNPC), salicin, and beechwood xylan (from China National Pharmaceutical Group Co., Ltd., Shanghai Yuanye Bio-Technology Co., Ltd., Shanghai, China) substrates dissolved with sodium-citrate buffer (0.05 M, pH 4.8) as previously described [37,62]. All assays were completed in independent triplicates.

Total proteins secreted by *T. reesei* were estimated as previously described [37]. The SDS-PAGE was run for profiling all proteins secreted by *T. reesei* using stain-free precast gels (Zoman Biotechnology Co., Ltd., Beijing, China), according to the manufacturer's instructions. All crude enzymes secreted by *T. reesei* were analyzed by LC-MS/MS (Jingjie PTM BioLab Co., Ltd., Hangzhou, China; Orbitrap Elite LC-MS/MS, Thermo, Waltham, MA, USA), as described in [37]. Liquid-chromatography-MS/MS-analysis data were identified by searching the *T. reesei* Rut-C30 protein-sequence databases downloaded from Uniprot (<https://www.uniprot.org/>), accessed on 30 April 2022.

3.9. Preparation of Biocarbon Materials

The remaining solid residue obtained from *T. reesei* cultivation with corn (ZH) stalk was mixed with FeCl_3 (1:2, w/w), and ground into the powder. The powder sample was loaded into a tube furnace (OTF-1200X-60UV, Kejing Material Technology Co., Ltd., Hefei, China), heated under N_2 at a rate of $5\text{ }^\circ\text{C}/\text{min}$ up to $1000\text{ }^\circ\text{C}$ for 2 h, and then cooled down to $300\text{ }^\circ\text{C}$ at a rate of $10\text{ }^\circ\text{C}/\text{min}$. After cooling to room temperature, the excess ferric ions from the samples were rinsed with 1 M of HCl aqueous solution for 6 h. Next, the carbon residues were rinsed with deionized water until reaching pH 7.0, and the remaining residues were treated by ethanol under ultrasound for 2 h in a sonicator, and dried as biocarbon materials.

3.10. Characterization of Porous Carbons

The biocarbon materials were observed under transmission electron microscope (TEM, JEM-2800, Tokyo, Japan) and analyzed by X-ray diffraction (XRD, Advance D8) and Raman spectrum (Thermo Scientific DXR, Waltham, MA, USA). The elements and binding energy of carbon materials were detected by X-ray photoelectron spectroscopy (XPS, Thermo Scientific K-Alpha, Waltham, MA, USA). Specific surface area and pore diameter were analyzed by Automated Surface Area and Porosity Analyzer (Micromeritics ASAP 2460, Norcross, GA, USA)

3.11. Measurement of Electrochemical Properties

The electrochemical properties of biocarbon materials were evaluated as previously described [45]. About 0.032 g of biocarbon materials, 0.004 g of Super-P, and 0.004 g of PTFE were mixed with ethanol as the dispersant. Biocarbon materials and PTFE acted as the active materials and binder, respectively. The working electrode was prepared by pressing the above mixture onto a current collector, which was nickel foam ($1\text{ cm} \times 1\text{ cm}$). The test was performed in 6 M of KOH with a three-electrode system, in which a Hg/HgO and a platinum plate were applied as the reference and counter electrodes, respectively.

Cyclic voltammetry (CV) and galvanostatic charge-discharge (GCD) were performed on a CHI660E electrochemical workstation to evaluate the electrochemical performance. The CV was performed at scan rates of $100\text{ mV}/\text{s}$, and GCD was carried out at current densities from 0.5–20 A/g. The specific capacitance (C, F/g) based on GCD test was calculated by the following formula: $C = I \times \Delta t / (m \times \Delta V)$. In this formula, I, Δt and ΔV represent for the discharging current (A), discharging time (s) and discharging voltage (V)

excluding the IR drop during the discharging process; m (g) is the mass of active material in the working electrode [63].

4. Conclusions

By performing optimal LHW pretreatment with corn stalks, this study found that 4% FeCl₃ co-supplement led to near-complete biomass saccharification for high levels of bioethanol, and all the enzyme-undigestible residues were applicable as active biosorbents for Cd adsorption. When incubating the corn stalks with *T. reesei* for the secretion of lignocellulose-degradation enzymes, the 0.05% FeCl₃ co-supplement increased the secreted-enzyme activities by 1.3–3.0-fold, and the undigested residue was further activated by the 1:2 FeCl₃ to generate highly porous and graphene-like carbon, which was applicable as a supercapacitor with specific capacitances raised by 3–12-fold. Hence, this study demonstrated that FeCl₃ is a universal catalyst for low-cost bioethanol and high-value bioproduction with zero biomass-waste release.

Supplementary Materials: The following supporting information can be downloaded at: <https://www.mdpi.com/article/10.3390/molecules28052060/s1>, Figure S1: General experimental procedures conducted in this study; Figure S2: Mass-balance analyses for biomass enzymatic saccharification and bioethanol production under optimal LHW pretreatment co-supplied with 4% FeCl₃ in two corn (ZX, ZH) stalks; Figure S3: SEM observation of lignocellulose residues after optimal LHW pretreatment co-supplied with 4% FeCl₃ in two corn (ZX, ZH) stalks; Figure S4: SDS-PAGE profiling of total soluble proteins secreted by *T. reesei* strain after incubation with raw stalk of corn (ZH) cultivar co-supplied with 0.05% FeCl₃; Figure S5: Cyclic-voltammetry curves and galvanostatic charge–discharge curves of the porous carbon generated by 1:2 (*w/w*) FeCl₃-activated thermal–chemical conversion of the lignocellulose residues (RE) from *T. reesei* incubation with raw ZH stalk co-supplied with 0.05% FeCl₃; Table S1: Characteristic chemical bonds of FT-IR spectra presented in Figure 2.

Author Contributions: J.L. methodology, completion of experiments, writing of draft; X.Z. completion of partial experiments; H.P. investigation, chemical analysis; T.L. editing, data analysis; P.L. and H.G. investigation, data analysis; Y.W. and J.T. supervision, data analysis; Q.L. and Z.Q. data analysis and editing; L.P. conceptualization, supervision, revision; T.X. supervision, finalization of manuscript. All authors have read and agreed to the published version of the manuscript.

Funding: This work was in part supported by the National Natural Science Foundation of China (32101701, 32170268, 32100214), National 111 Project of Ministry of Education of China (BP0820035, D17009), and Opening Fund of Key Laboratory of Forage and Endemic Crop Biology, Ministry of Education (FECBOF2021005).

Institutional Review Board Statement: Not applicable.

Informed Consent Statement: Not applicable.

Data Availability Statement: Not applicable.

Conflicts of Interest: The authors declare no conflict of interest.

References

1. Ragauskas, A.J.; Williams, C.K.; Davison, B.H.; Britovsek, G.; Cairney, J.; Eckert, C.A.; Frederick, W.J.; Hallett, J.P.; Leak, D.J.; Liotta, C.L.; et al. The path forward for biofuels and biomaterials. *Science* **2006**, *311*, 484–489. [CrossRef]
2. Rubin, E.M. Genomics of cellulosic biofuels. *Nature* **2008**, *454*, 841–845. [CrossRef]
3. Carroll, A.; Somerville, C. Cellulosic Biofuels. *Annu. Rev. Plant Biol.* **2009**, *60*, 165–182. [CrossRef]
4. Wang, Y.; Fan, C.; Hu, H.; Li, Y.; Sun, D.; Wang, Y.; Peng, L. Genetic modification of plant cell walls to enhance biomass yield and biofuel production in bioenergy crops. *Biotechnol. Adv.* **2016**, *34*, 997–1017. [CrossRef]
5. Lynd, L.R.; Beckham, G.T.; Guss, A.M.; Jayakody, L.N.; Karp, E.M.; Maranas, C.; McCormick, R.L.; Amador-Noguez, D.; Bomble, Y.J.; Davison, B.H.; et al. Toward low-cost biological and hybrid biological/catalytic conversion of cellulosic biomass to fuels. *Energy Environ. Sci.* **2022**, *15*, 938–990. [CrossRef]
6. Yoo, C.G.; Meng, X.; Pu, Y.; Ragauskas, A.J. The critical role of lignin in lignocellulosic biomass conversion and recent pretreatment strategies: A comprehensive review. *Bioresour. Technol.* **2020**, *301*, 122784. [CrossRef]
7. Li, Y.; Liu, P.; Huang, J.; Zhang, R.; Hu, Z.; Feng, S.; Wang, Y.; Wang, L.; Xia, T.; Peng, L. Mild chemical pretreatments are sufficient for bioethanol production in transgenic rice straws overproducing glucosidase. *Green Chem.* **2018**, *20*, 2047–2056. [CrossRef]

8. Sun, D.; Yang, Q.; Wang, Y.; Gao, H.; He, M.; Lin, X.; Lu, J.; Wang, Y.; Kang, H.; Alam, A.; et al. Distinct mechanisms of enzymatic saccharification and bioethanol conversion enhancement by three surfactants under steam explosion and mild chemical pretreatments in bioenergy *Miscanthus. Ind. Crops Prod.* **2020**, *153*, 112559. [[CrossRef](#)]
9. Chen, W.-H.; Nižetić, S.; Sirohi, R.; Huang, Z.; Luque, R.M.; Papadopoulos, A.; Sakthivel, R.; Phuong Nguyen, X.; Tuan Hoang, A. Liquid hot water as sustainable biomass pretreatment technique for bioenergy production: A review. *Bioresour. Technol.* **2022**, *344*, 126207. [[CrossRef](#)]
10. Wells, J.M.; Driellak, E.; Surendra, K.C.; Kumar Khanal, S. Hot water pretreatment of lignocellulosic biomass: Modeling the effects of temperature, enzyme and biomass loadings on sugar yield. *Bioresour. Technol.* **2020**, *300*, 122593. [[CrossRef](#)]
11. Novy, V.; Nielsen, F.; Seiboth, B.; Nidetzky, B. The influence of feedstock characteristics on enzyme production in *Trichoderma reesei*: A review on productivity, gene regulation and secretion profiles. *Biotechnol. Biofuels* **2019**, *12*, 238. [[CrossRef](#)]
12. Kang, K.; Wang, S.; Lai, G.; Liu, G.; Xing, M. Characterization of a novel swollenin from *Penicillium oxalicum* in facilitating enzymatic saccharification of cellulose. *BMC Biotechnol.* **2013**, *13*, 42. [[CrossRef](#)]
13. Wang, P.; Zhang, G.; Wei, X.-Y.; Liu, R.; Gu, J.-J.; Cao, F.-F. Bioselective Synthesis of a Porous Carbon Collector for High-Performance Sodium-Metal Anodes. *J. Am. Chem. Soc.* **2021**, *143*, 3280–3283. [[CrossRef](#)]
14. Lizundia, E.; Luzzi, F.; Puglia, D. Organic waste valorisation towards circular and sustainable biocomposites. *Green Chem.* **2022**, *24*, 5429–5459. [[CrossRef](#)]
15. Chakraborty, R.; Vilya, K.; Pradhan, M.; Nayak, A.K. Recent advancement of biomass-derived porous carbon based materials for energy and environmental remediation applications. *J. Mater. Chem. A* **2022**, *10*, 6965–7005. [[CrossRef](#)]
16. Deng, J.; Li, M.; Wang, Y. Biomass-derived carbon: Synthesis and applications in energy storage and conversion. *Green Chem.* **2016**, *18*, 4824–4854. [[CrossRef](#)]
17. Dong, J.; Li, S.; Ding, Y. Anchoring nickel-cobalt sulfide nanoparticles on carbon aerogel derived from waste watermelon rind for high-performance asymmetric supercapacitors. *J. Alloys Compd.* **2020**, *845*, 155701. [[CrossRef](#)]
18. Zou, K.; Deng, Y.; Wu, W.; Zhang, S.; Chen, G. A novel eutectic solvent precursor for efficiently preparing N-doped hierarchically porous carbon nanosheets with unique surface functional groups and micropores towards dual-carbon lithium-ion capacitors. *J. Mater. Chem. A* **2021**, *9*, 13631–13641. [[CrossRef](#)]
19. Zhang, G.; Liu, X.; Wang, L.; Fu, H. Recent advances of biomass derived carbon-based materials for efficient electrochemical energy devices. *J. Mater. Chem. A* **2022**, *10*, 9277–9307. [[CrossRef](#)]
20. Tejirian, A.; Xu, F. Inhibition of Cellulase-Catalyzed Lignocellulosic Hydrolysis by Iron and Oxidative Metal Ions and Complexes. *Appl. Environ. Microbiol.* **2010**, *76*, 7673–7682. [[CrossRef](#)]
21. Rodriguez, J.; Ferraz, A.; de Mello, M.P. Role of Metals in Wood Biodegradation. In *Wood Deterioration and Preservation*; American Chemical Society: Washington, DC, USA, 2003; Volume 845, pp. 154–174.
22. Huang, L.; Forsberg, C.W.; Thomas, D.Y. Purification and characterization of a chloride-stimulated cellobiosidase from *Bacteroides succinogenes* S85. *J. Bacteriol.* **1988**, *170*, 2923–2932. [[CrossRef](#)]
23. Zhao, Y.; Damgaard, A.; Christensen, T.H. Bioethanol from corn stover—A review and technical assessment of alternative biotechnologies. *Prog. Energy Combust. Sci.* **2018**, *67*, 275–291. [[CrossRef](#)]
24. Kamireddy, S.R.; Li, J.B.; Tucker, M.; Degenstein, J.; Ji, Y. Effects and Mechanism of Metal Chloride Salts on Pretreatment and Enzymatic Digestibility of Corn Stover. *Ind. Eng. Chem. Res.* **2013**, *52*, 1775–1782. [[CrossRef](#)]
25. Yu, H.; Hu, M.; Hu, Z.; Liu, F.; Yu, H.; Yang, Q.; Gao, H.; Xu, C.; Wang, M.; Zhang, G.; et al. Insights into pectin dominated enhancements for elimination of toxic Cd and dye coupled with ethanol production in desirable lignocelluloses. *Carbohydr. Polym.* **2022**, *286*, 119298. [[CrossRef](#)]
26. Guo, H.P.; Hong, C.T.; Chen, X.M.; Xu, Y.X.; Liu, Y.; Jiang, D.A.; Zheng, B.S. Different Growth and Physiological Responses to Cadmium of the Three *Miscanthus* Species. *PLoS ONE* **2016**, *11*, e0153475. [[CrossRef](#)]
27. Xu, F.; Yu, J.M.; Tesso, T.; Dowell, F.; Wang, D.H. Qualitative and quantitative analysis of lignocellulosic biomass using infrared techniques: A mini-review. *Appl. Energy* **2013**, *104*, 801–809. [[CrossRef](#)]
28. Ong, H.C.; Chen, W.H.; Singh, Y.; Gan, Y.Y.; Chen, C.Y.; Show, P.L. A state-of-the-art review on thermochemical conversion of biomass for biofuel production: A TG-FTIR approach. *Energy Convers. Manag.* **2020**, *209*, 11264. [[CrossRef](#)]
29. Pancholi, M.J.; Khristi, A.; Athira, K.M.; Bagchi, D. Comparative Analysis of Lignocellulose Agricultural Waste and Pre-treatment Conditions with FTIR and Machine Learning Modeling. *BioEnergy Res.* **2022**. [[CrossRef](#)]
30. Sammons, R.J.; Harper, D.P.; Labbe, N.; Bozell, J.J.; Elder, T.; Rials, T.G. Characterization of Organosolv Lignins using Thermal and FT-IR Spectroscopic Analysis. *BioResources* **2013**, *8*, 2752–2767. [[CrossRef](#)]
31. Zhuang, J.; Li, M.; Pu, Y.; Ragauskas, A.J.; Yoo, C.G. Observation of Potential Contaminants in Processed Biomass Using Fourier Transform Infrared Spectroscopy. *Appl. Sci.* **2020**, *10*, 4345. [[CrossRef](#)]
32. Alvira, P.; Tomás-Pejó, E.; Ballesteros, M.; Negro, M.J. Pretreatment technologies for an efficient bioethanol production process based on enzymatic hydrolysis: A review. *Bioresour. Technol.* **2010**, *101*, 4851–4861. [[CrossRef](#)]
33. Funahashi, R.; Ono, Y.; Tanaka, R.; Yokoi, M.; Daido, K.; Inamochi, T.; Saito, T.; Horikawa, Y.; Isogai, A. Changes in the degree of polymerization of wood celluloses during dilute acid hydrolysis and TEMPO-mediated oxidation: Formation mechanism of disordered regions along each cellulose microfibril. *Int. J. Biol. Macromol.* **2018**, *109*, 914–920. [[CrossRef](#)]
34. Zhou, X.; Xu, Z.; He, J.; Li, Y.; Pan, C.; Wang, C.; Deng, M.-R.; Zhu, H. A myxobacterial LPMO10 has oxidizing cellulose activity for promoting biomass enzymatic saccharification of agricultural crop straws. *Bioresour. Technol.* **2020**, *318*, 124217. [[CrossRef](#)]

35. Pihlajaniemi, V.; Sipponen, M.H.; Liimatainen, H.; Sirviö, J.A.; Nyyssölä, A.; Laakso, S. Weighing the factors behind enzymatic hydrolyzability of pretreated lignocellulose. *Green Chem.* **2016**, *18*, 1295–1305. [[CrossRef](#)]
36. Xu, C.; Zhu, J.; Yu, H.; Yu, H.; Yang, Y.; Fu, Q.; Zhan, D.; Wang, Y.; Wang, H.; Zhang, Y.; et al. Recyclable cascading of arsenic phytoremediation and lead removal coupled with high bioethanol production using desirable rice straws. *Biochem. Eng. J.* **2021**, *168*, 107950. [[CrossRef](#)]
37. Liu, P.; Li, A.; Wang, Y.; Cai, Q.; Yu, H.; Li, Y.; Peng, H.; Li, Q.; Wang, Y.; Wei, X.; et al. Distinct *Miscanthus* lignocellulose improves fungus secreting cellulases and xylanases for consistently enhanced biomass saccharification of diverse bioenergy crops. *Renew. Energy* **2021**, *174*, 799–809. [[CrossRef](#)]
38. Peng, H.; Zhao, W.; Liu, J.; Liu, P.; Yu, H.; Deng, J.; Yang, Q.; Zhang, R.; Hu, Z.; Liu, S.; et al. Distinct cellulose nanofibrils generated for improved Pickering emulsions and lignocellulose-degradation enzyme secretion coupled with high bioethanol production in natural rice mutants. *Green Chem.* **2022**, *24*, 2975–2987. [[CrossRef](#)]
39. Chen, L.; Zou, G.; Wang, J.; Wang, J.; Liu, R.; Jiang, Y.; Zhao, G.; Zhou, Z. Characterization of the Ca²⁺-responsive signaling pathway in regulating the expression and secretion of cellulases in *Trichoderma reesei* Rut-C30. *Mol. Microbiol.* **2016**, *100*, 560–575. [[CrossRef](#)]
40. Chen, Y.; Shen, Y.; Wang, W.; Wei, D. Mn²⁺ modulates the expression of cellulase genes in *Trichoderma reesei* Rut-C30 via calcium signaling. *Biotechnol. Biofuels* **2018**, *11*, 54. [[CrossRef](#)]
41. Yenenler, A.; Kurt, H.; Sezerman, O.U. Enhancing Enzymatic Properties of Endoglucanase I Enzyme from *Trichoderma reesei* via Swapping from Cellobiohydrolase I Enzyme. *Catalysts* **2019**, *9*, 130. [[CrossRef](#)]
42. Arampatzidou, A.C.; Deliyanni, E.A. Comparison of activation media and pyrolysis temperature for activated carbons development by pyrolysis of potato peels for effective adsorption of endocrine disruptor bisphenol-A. *J. Colloid Interface Sci.* **2016**, *466*, 101–112. [[CrossRef](#)]
43. Ferrari, A.C.; Robertson, J. Interpretation of Raman spectra of disordered and amorphous carbon. *Phys. Rev. B* **2000**, *61*, 14095–14107. [[CrossRef](#)]
44. Kim, J.B.; Koo, S.H.; Kim, I.H.; Kim, J.T.; Kim, J.G.; Jayaraman, B.; Lim, J.; Kim, S.O. Characteristic dual-domain composite structure of reduced graphene oxide and its application to higher specific capacitance. *Chem. Eng. J.* **2022**, *446*, 137390. [[CrossRef](#)]
45. Wang, P.; Zhang, G.; Li, M.-Y.; Yin, Y.-X.; Li, J.-Y.; Li, G.; Wang, W.-P.; Peng, W.; Cao, F.-F.; Guo, Y.-G. Porous carbon for high-energy density symmetrical supercapacitor and lithium-ion hybrid electrochemical capacitors. *Chem. Eng. J.* **2019**, *375*, 122020. [[CrossRef](#)]
46. Kong, X.; Zhu, Y.; Lei, H.; Wang, C.; Zhao, Y.; Huo, E.; Lin, X.; Zhang, Q.; Qian, M.; Mateo, W.; et al. Synthesis of graphene-like carbon from biomass pyrolysis and its applications. *Chem. Eng. J.* **2020**, *399*, 125808. [[CrossRef](#)]
47. Wang, Y.; Rong, Z.; Wang, Y.; Wang, T.; Du, Q.; Wang, Y.; Qu, J. Graphene-Based Metal/Acid Bifunctional Catalyst for the Conversion of Levulinic Acid to γ -Valerolactone. *ACS Sustain. Chem. Eng.* **2017**, *5*, 1538–1548. [[CrossRef](#)]
48. Chen, Z.; Liao, S.; Ge, L.; Amaniampong, P.N.; Min, Y.; Wang, C.; Li, K.; Lee, J.-M. Reduced graphene oxide with controllably intimate bifunctionality for the catalytic transformation of fructose into 2,5-diformylfuran in biphasic solvent systems. *Chem. Eng. J.* **2020**, *379*, 122284. [[CrossRef](#)]
49. Lakmini, L.M.N.; Deshan, A.D.K.; Pham, H.D.; Doherty, W.; Rackemann, D.; Dubal, D.P.; Moghaddam, L. High carbon utilization: 5-(Chloromethyl)furfural (CMF) production from rice by-products and transformation of CMF residues into Li-ion energy storage systems. *J. Clean. Prod.* **2022**, *375*, 134082. [[CrossRef](#)]
50. Xie, Z.; Shang, X.; Yan, J.; Hussain, T.; Nie, P.; Liu, J. Biomass-derived porous carbon anode for high-performance capacitive deionization. *Electrochim. Acta* **2018**, *290*, 666–675. [[CrossRef](#)]
51. Yumak, T.; Yakaboylu, G.A.; Oginni, O.; Singh, K.; Ciftiyurek, E.; Sabolsky, E.M. Comparison of the electrochemical properties of engineered switchgrass biomass-derived activated carbon-based EDLCs. *Colloids Surf. A Physicochem. Eng. Asp.* **2020**, *586*, 124150. [[CrossRef](#)]
52. Peng, L.; Hocart, C.H.; Redmond, J.W.; Williamson, R.E. Fractionation of carbohydrates in *Arabidopsis* root cell walls shows that three radial swelling loci are specifically involved in cellulose production. *Planta* **2000**, *211*, 406–414. [[CrossRef](#)]
53. Li, F.; Xie, G.; Huang, J.; Zhang, R.; Li, Y.; Zhang, M.; Wang, Y.; Li, A.; Li, X.; Xia, T.; et al. OsCESA9 conserved-site mutation leads to largely enhanced plant lodging resistance and biomass enzymatic saccharification by reducing cellulose DP and crystallinity in rice. *Plant Biotechnol. J.* **2017**, *15*, 1093–1104. [[CrossRef](#)]
54. Wu, Z.; Zhang, M.; Wang, L.; Tu, Y.; Zhang, J.; Xie, G.; Zou, W.; Li, F.; Guo, K.; Li, Q.; et al. Biomass digestibility is predominantly affected by three factors of wall polymer features distinctive in wheat accessions and rice mutants. *Biotechnol. Biofuels* **2013**, *6*, 183. [[CrossRef](#)]
55. Alam, A.; Zhang, R.; Liu, P.; Huang, J.; Wang, Y.; Hu, Z.; Madadi, M.; Sun, D.; Hu, R.; Ragauskas, A.J.; et al. A finalized determinant for complete lignocellulose enzymatic saccharification potential to maximize bioethanol production in bioenergy *Miscanthus*. *Biotechnol. Biofuels* **2019**, *12*, 99. [[CrossRef](#)]
56. Wiman, M.; Dienes, D.; Hansen, M.A.T.; van der Meulen, T.; Zacchi, G.; Lidén, G. Cellulose accessibility determines the rate of enzymatic hydrolysis of steam-pretreated spruce. *Bioresour. Technol.* **2012**, *126*, 208–215. [[CrossRef](#)]
57. Wang, Y.; Huang, J.; Li, Y.; Xiong, K.; Wang, Y.; Li, F.; Liu, M.; Wu, Z.; Tu, Y.; Peng, L. Ammonium oxalate-extractable uronic acids positively affect biomass enzymatic digestibility by reducing lignocellulose crystallinity in *Miscanthus*. *Bioresour. Technol.* **2015**, *196*, 391–398. [[CrossRef](#)]

58. Wu, L.; Feng, S.; Deng, J.; Yu, B.; Wang, Y.; He, B.; Peng, H.; Li, Q.; Hu, R.; Peng, L. Altered carbon assimilation and cellulose accessibility to maximize bioethanol yield under low-cost biomass processing in corn brittle stalk. *Green Chem.* **2019**, *21*, 4388–4399. [[CrossRef](#)]
59. Jin, W.; Chen, L.; Hu, M.; Sun, D.; Li, A.; Li, Y.; Hu, Z.; Zhou, S.; Tu, Y.; Xia, T.; et al. Tween-80 is effective for enhancing steam-exploded biomass enzymatic saccharification and ethanol production by specifically lessening cellulase absorption with lignin in common reed. *Appl. Energy* **2016**, *175*, 82–90. [[CrossRef](#)]
60. Liu, F.; Li, J.; Yu, H.; Li, Y.; Wang, Y.; Gao, H.; Peng, H.; Hu, Z.; Wang, H.; Zhang, G.; et al. Optimizing two green-like biomass pretreatments for maximum bioethanol production using banana pseudostem by effectively enhancing cellulose depolymerization and accessibility. *Sustain. Energy Fuels* **2021**, *5*, 3467–3478. [[CrossRef](#)]
61. Yu, J.-x.; Wang, L.-y.; Chi, R.-a.; Zhang, Y.-f.; Xu, Z.-g.; Guo, J. Adsorption of Pb^{2+} , Cd^{2+} , Cu^{2+} , and Zn^{2+} from aqueous solution by modified sugarcane bagasse. *Res. Chem. Intermed.* **2015**, *41*, 1525–1541. [[CrossRef](#)]
62. Song, W.; Han, X.; Qian, Y.; Liu, G.; Yao, G.; Zhong, Y.; Qu, Y. Proteomic analysis of the biomass hydrolytic potentials of *Penicillium oxalicum* lignocellulolytic enzyme system. *Biotechnol. Biofuels* **2016**, *9*, 68. [[CrossRef](#)]
63. Oyedotun, K.O.; Barzegar, F.; Mirghni, A.A.; Khaleed, A.A.; Masikhwa, T.M.; Manyala, N. Examination of High-Porosity Activated Carbon Obtained from Dehydration of White Sugar for Electrochemical Capacitor Applications. *ACS Sustain. Chem. Eng.* **2019**, *7*, 537–546. [[CrossRef](#)]

Disclaimer/Publisher’s Note: The statements, opinions and data contained in all publications are solely those of the individual author(s) and contributor(s) and not of MDPI and/or the editor(s). MDPI and/or the editor(s) disclaim responsibility for any injury to people or property resulting from any ideas, methods, instructions or products referred to in the content.